Composites Science and Technology 249 (2024) 110503

Contents lists available at ScienceDirect

Composites Science and Technology

journal homepage: www.elsevier.com/locate/compscitech

4D printed bio-inspired mesh composite materials with high stretchability and reconfigurability

Chengjun Zeng [a], Liwu Liu [a], Xiaozhou Xin [a], Wei Zhao [a], Cheng Lin [b], Yanju Liu [a,**], Jinsong Leng [b,*]

[a] Department of Astronautical Science and Mechanics, Harbin Institute of Technology (HIT), Harbin, 150001, Heilongjiang, China
[b] Center for Composite Materials and Structures, Harbin Institute of Technology (HIT), Harbin, 150080, Heilongjiang, China

ARTICLE INFO

Keywords:
Stretchability
4D printing
Mesh composites
Flexible electronics
Shape memory polymers

ABSTRACT

Strain engineering such as Kirigami design offers viable solutions for transforming rigid or even non-stretchable materials into highly stretchable structures, thus providing new opportunities for building flexible electronic devices with biological tissue-like mechanical properties. However, the stretchability of stretchable structures based on traditional Kirigami design strategies often relies on out-of-plane deformation, thus posing a great challenge for flexible electronic devices with high planarity requirements. Moreover, the low modulus properties of conventional soft materials also put forward new requirements for flexible electronic devices with complex mechanical environment adaptability. Here, Kirigami-like mesh composite materials (MCMs) based on shape memory polymer (SMP) and continuous carbon fibers, inspired by the laminar layout pattern of biological collagen tissues, were proposed and fabricated by 4D printing. 4D printed MCMs achieve elongation only through in-plane deformation and can combine excellent mechanical properties with high stretchability. The customizable fiber orientation enables MCMs with tunable stretchability from 1.8% to 375% and tensile modulus spanning four orders of magnitude from 0.04 MPa to 1375 MPa. In addition, owing to the variable stiffness properties and shape memory effect of SMP, it is also possible to achieve tunable stretchability and mechanical properties of MCMs with predetermined fiber orientation by controlling the ambient temperature, which facilitates the design of flexible electronic devices that conform to complex thermodynamic environments.

1. Introduction

Over the past two decades, the emerging field of flexible electronics based on soft materials has made unprecedented progress [1–3]. Due to their mechanical properties close to those of biological tissues, flexible electronic devices can minimize the mechanical mismatch at the biotic–abiotic interface and thus have promising applications in areas such as smart electronic skins, wearable communication products, bionic digital cameras, and biomedical devices [4–6]. The most attractive property introduced in emerging flexible electronic devices is the high stretchability without sacrificing the extreme mechanical load-bearing capacity of devices [7]. Currently, two strategies including material innovation and strain engineering have been used to achieve stretchability in flexible electronic devices [8]. The former strategy requires the identification and development of novel soft materials capable of withstanding inherent in-plane strains, which often possess large deformation capabilities and enhanced electromechanical features, such as organic/inorganic composites, eutectic alloys, and conductive organic networks [9–11]. Many electronic devices designed using this strategy have attractive properties including high stretchability and fast self-healing, such as supercapacitors [12], organogel-based triboelectric nanogenerators (TENG) [13], human motion sensors [14] and wearable thermal-electric harvester [15].

On the other hand, the strain engineering strategy frees the design ideas of flexible electronics from the material innovation arena and extends the available materials to rigid or even completely non-stretchable materials [16]. This strategy not only addresses the difference in mechanical properties between biological and non-biological interfaces, but also allows easy conversion between planar and non-planar configurations. Prevailing strain engineering paradigms can be classified into wavy/wrinkle, island-bridge, Kirigami, and nanomesh [17]. Mechanically buckling-induced wavy/wrinkle is an early

* Corresponding author.
** Corresponding author.
E-mail addresses: yj_liu@hit.edu.cn (Y. Liu), lengjs@hit.edu.cn (J. Leng).

https://doi.org/10.1016/j.compscitech.2024.110503
Received 2 November 2023; Received in revised form 6 December 2023; Accepted 13 February 2024
Available online 15 February 2024

developed strain engineering strategy to deposit electronic materials on pre-stretched flexible substrates and then obtain stretchable electronic devices through the release of pre-strain, whose stretchability can be as high as several hundred percent [7]. The Kirigami design strategy, inspired by the art of papercutting, possesses the ability to combine in-plane stretching and out-of-plane buckling to build 3D configurations, thus becoming a novel avenue for the development of flexible electronics [18]. This strategy is achieved by introducing rationally designed cutting patterns in the intact film to split it into several stretchable parts [19,20]. However, the stretchability of flexible electronic devices based on the Kirigami design strategy often relies on out-of-plane deformation, and such non-planar features may significantly increase surface roughness and lead to poor adhesion, thus posing a great challenge for flexible devices that require smooth surfaces [21].

Recently, paradigms have been developed to incorporate programmable and reconfigurable mechanisms into flexible electronic devices through 4D printing [22–24]. Based on the strain engineering strategy, 4D printing enables the integrated fabrication of stretchable structures with active and reversible deformation characteristics by assembling stimuli-responsive materials layer by layer [25,26]. For example, Zhang et al. [27] layered shape memory polymers (SMPs) and conductive paste by 4D printing to seamlessly integrate stretchable heating circuits with fractal patterns. Zhou et al. [28] prepared stretchable electrodes with arbitrary shapes by 4D printing of conductive composites. However, these efforts to endow flexible electronics with active deformability through 4D printing rely on composite inks or soft materials, whose low modulus properties are difficult to meet the requirements imposed on flexible electronics by complex mechanical environments.

Some biological collagen fibrous tissues such as cortical bone are typically hierarchical biomaterials whose microstructure is composed of a layered arrangement of lamellae with varying fibril orientation [29]. Inspired by the laminar layout pattern (Fig. 1a) and the strain engineering paradigm based on the Kirigami, we report a design strategy for multilayer mesh composite materials (MCMs) as shown in Fig. 1b. The out-of-plane deformation during the stretching process is eliminated as much as possible by means of cross-plying of fibrous ligaments without sacrificing the stretchable capability of the Kirigami structure.

Two predetermined fiber angles α and θ are used as key parameters to control the tailorability of the mesh configuration. The designable fiber orientation enables MCMs with tunable stretchability from 1.8% to 375% and customizable tensile modulus from 0.04 MPa to 1375 MPa. The temperature sensitivity of SMP confers thermotropic variable stiffness capability to MCMs with predetermined fiber orientations, and elevated temperatures substantially develop the stretchability and toughness of MCMs. The anisotropic viscoelasticity theory of shape memory polymer composites (SMPCs) is implemented in the commercial finite element software ABAQUS through the User Materials (UMAT) subroutine to simulate the tensile behavior and shape memory effect of MCMs. Finally, light-emitting diode (LED) integrated devices demonstrate the potential application of 4D printed stretchable MCMs in flexible electronic devices.

2. Experimental section

2.1. Materials

The thermoplastic polymer used in the printing process is polylactic acid (PLA)-based SMP and the continuous fiber is Toray T300B-1000 carbon fiber. The glass transition temperature and melting temperature of PLA-based SMP are 336 K and 443 K, respectively [30]. The LEDs and conductive silver paste used to fabricate MCM-based LED systems are 1206 SMD-LEDs and Conduction CD-03 silver paste, respectively, where the viscosity of the Conduction CD-03 silver paste was about 1.9 $\times$ 10^5 CPS.

2.2. Specimen fabrication

The detailed design of the MCMs is presented in Fig. S1a. Besides the

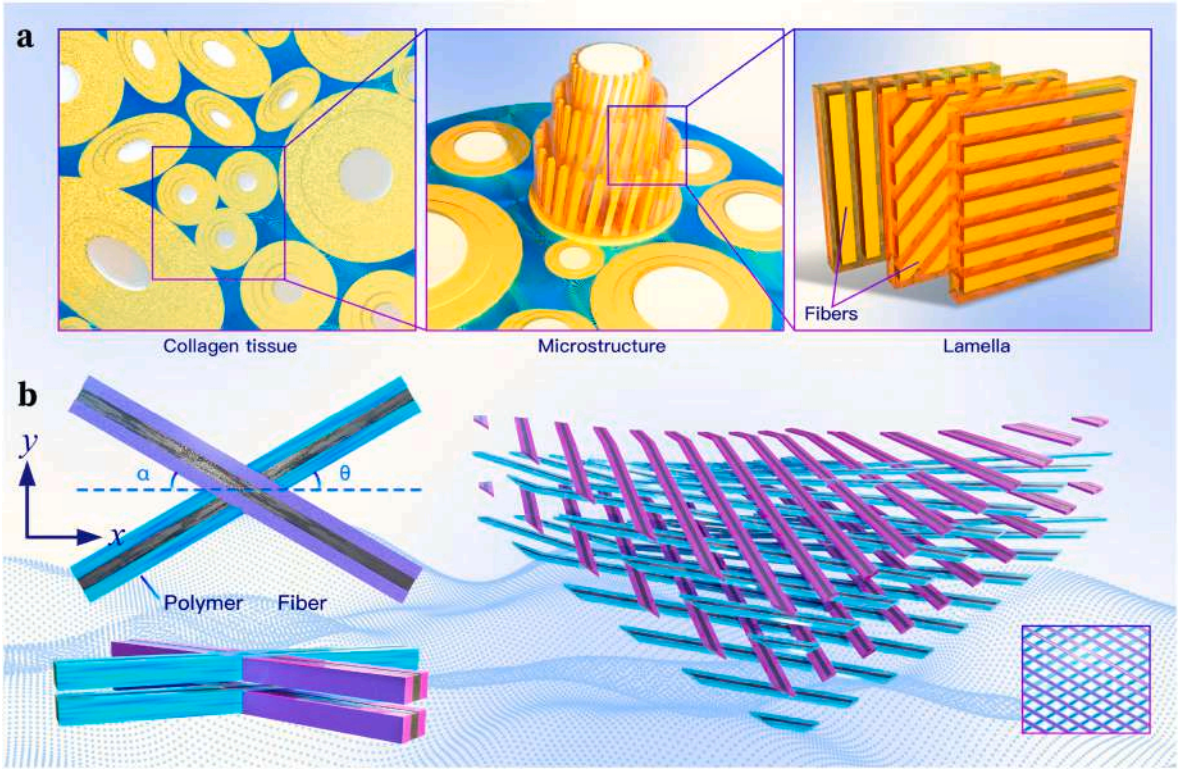

Fig. 1. Design and fabrication of bio-inspired MCMs. (**a**) Schematic illustration of the microstructure and laminar structure of the biological collagen tissue. (**b**) Design of bio-inspired and Kirigami-like multilayer MCMs.

fiber angles α and θ, the geometric characteristics of the MCMs are further delineated by parameters such as the fibrous ligament spacing w and the fibrous ligament width t. In this study, the spacing of the adjacent fibrous ligaments and fibrous ligament width were set at $w = 10$ mm and $t = 1.5$ mm, respectively. Moreover, the length, width, and out-of-plane thickness of the effective mesh segment for all MCM samples were $h = 100$ mm, $l = 100$ mm, and $b = 0.6$ mm, respectively. Digital fabrication of MCMs was achieved by a commercial composite 3D printer (Combot-200, Shaanxi Fibertech Technology Development Co., Ltd., China) based on the in-situ melt coextrusion principle of continuous fibers/thermoplastic polymers. Continuous printing paths that match target samples were planned to ensure that no nozzle skipping occurs during printing. The printing speed and nozzle temperature for all samples were respectively set to 100 mm/min and 493 K to obtain a trade-off between printing accuracy and efficiency. To obtain an out-of-plane thickness of 0.6 mm, two deposited layers were superimposed, where each layer has a thickness of 0.3 mm. The fibrous ligament width was regulated by planning the feeding rate and the outer diameter of the nozzle. In this work, three α values (0°, 30° and 60°) and nine θ values (10°–90° with 10° interval) are selected to construct the target samples. The fabrication process of a typical MCM sample and photographs of several printed samples are shown in Figs. S1b and S1c, respectively. It is worth mentioning that the printed prototypes need to be mechanically cut to obtain MCM samples that meet the design dimensions.

2.3. Mechanical testing of MCMs

Uniaxial tensile tests of 4D printed MCMs under three isothermal conditions, 298 K, 318 K, and 338 K, were performed on an electronic universal testing machine (ZwickRoell Z010) equipped with an environmental chamber. A loading rate of 10 mm/min was used to apply a strain rate of 0.17%. Engineering stress-strain curves were recorded, and the mean and standard deviation of mechanical properties such as stretchability, tensile modulus, ultimate tensile strength, and toughness were extracted from three identical samples for each test.

2.4. Shape memory performance testing of MCMs

Shape programming and shape recovery tests of 4D printed MCMs were carried out in a hot water bath at 343 K. Samples were firstly heated at 343 K for 5 min, and then an axial displacement of 25 mm was applied to program them into a temporary shape. Samples were cooled to room temperature and the load was released to fix their temporary configurations while maintaining the axial displacement. Finally, samples with temporary configurations were heated at 343 K and the shape recovery process was observed.

2.5. Integration and demonstration of MCM-based LED systems

Several LEDs were connected in series and fixed on the surface of 4D printed MCM substrate, and the conductive silver paste was printed to form a conducting circuit. An external 12 V DC power supply was manipulated to light the LEDs.

2.6. Finite element simulation

An anisotropic viscoelastic constitutive model was developed as the theoretical basis for finite element simulation of 4D printed MCMs. The detailed derivation of the theoretical model can be found in *Supplementary Information*. Based on the developed theoretical model, a UMAT subroutine was written and implemented into ABAQUS to realize the finite element simulation for the uniaxial tensile behavior and shape memory effect (4D transformation) of MCMs. MCMs were meshed with twenty-node quadratic hexahedral elements (C3D20R). All simulations were performed in a quasi-static manner and geometric nonlinearities were incorporated. The finite element simulation for the shape memory cycling of MCMs is divided into the following four steps. Step 1 (S1): The sample was subjected to the maximum strain ε_{max} ($\varepsilon_{max} = 0.05$, 0.15, and 0.25) at 343 K. Step 2 (S2): The sample is cooled to 298 K while keeping the sample in a stretched state. Step 3 (S3): The load is unloaded at 298 K. Step 4 (S4): The sample is heated to 343 K without load.

3. Results and discussion

3.1. Tailorable stretchability and mechanical properties of MCMs

The parallelogram-like mesh design strategy controlled by the geometric parameters α and θ provides the structure with tailorable stretchability and mechanical properties. Fig. 2a-c depict the engineering stress-strain curves for 4D printed MCMs with fiber angle $\alpha = 0°$ at various θ. The engineering stress is defined as $\sigma = F/S$, where F and S respectively represent the tensile force and equivalent cross-sectional area. The equivalent cross-sectional area is expressed as $S = l \times b$. The engineering strain is defined as $\varepsilon = u/h$, where u and h are the loading displacement and initial length of the effective mesh segment of the MCM, respectively. A preliminary observation is that the maximum strength gradually increases and the strain at break gradually decreases as the fiber angle θ increases.

Fig. 2d plots the stretchability versus θ, from which it can be found that the stretchability of MCMs is strongly negatively correlated with θ. MCMs exhibit an inextensibility close to that of carbon fiber at $\theta = 90°$ and an extremely large stretchability of 375% at $\theta = 10°$. Over 200 times stretchability variation offers an extremely wide tailorable range of elongation. Moreover, the tailorable range of elongation covers the stretchability of common stretchable structures such as wavy/wrinkle [31], nanomesh [32] and Kirigami structures [8]. Therefore, MCMs offer satisfactory selectivity for flexible electronic devices with customized stretchability requirements. The structure-based tailorable mechanical properties such as tensile modulus, tensile strength and toughness are additional advantages of 4D printed MCMs. Fig. 2e-g presents the evolution of tensile modulus, tensile strength and toughness with θ, respectively, from which it can be concluded that the tensile modulus and tensile strength increase monotonically with θ. Customizable fiber orientation θ enables four orders of magnitude change in tensile modulus from 0.04 MPa to 1375 MPa. The tunable tensile modulus and tensile strength ranges of MCMs cover the mechanical property boundaries of natural biomaterials such as skin [33] and skeletal muscle [34].

To more fully demonstrate the biomechanical compatibility of MCMs, we derived material-property charts that can describe the multidimensional mechanical properties of the materials, as shown in Fig. 2h and i. In the two-dimensional mapping with stretchability and tensile modulus as axes, the curve representing MCMs runs through the regions of natural biomaterials such as tendons [35], skins [33], articular cartilage [36], liver capsule [37], gastrointestinal tract [35], and nerve [38], indicating that it is possible to obtain MCMs with mechanical properties matching these biomaterials by modulating the structural parameters, thus showing the promising application of MCMs in the field of bio-flexible electronic devices.

As another structural parameter, α can also significantly affect the mechanical properties of MCMs. Here we systematically investigate the coupling effects of α and θ on the tensile properties of MCMs. The tensile curves of MCMs at $\alpha = 30°$ for different θ exhibit similar evolutionary trends to those at $\alpha = 0°$ (Fig. S2). The main difference is that the MCM with $\alpha = 30°$ has higher ultimate strength and less stretchability than the MCM with $\alpha = 0°$ for the same θ. Compared to MCMs with $\alpha = 0°$ or $\alpha = 30°$, MCMs with $\alpha = 60°$ possess significantly increased ultimate strength for the same θ (Fig. S3). Fig. S4 exhibits the coupled influence of two structural parameters α and θ on the stretchability, tensile modulus and tensile strength in the form of 3D histograms. Consistent with the previous analysis, increasing the values of α and θ will contribute large tensile modulus and strength to the structure at the expense of

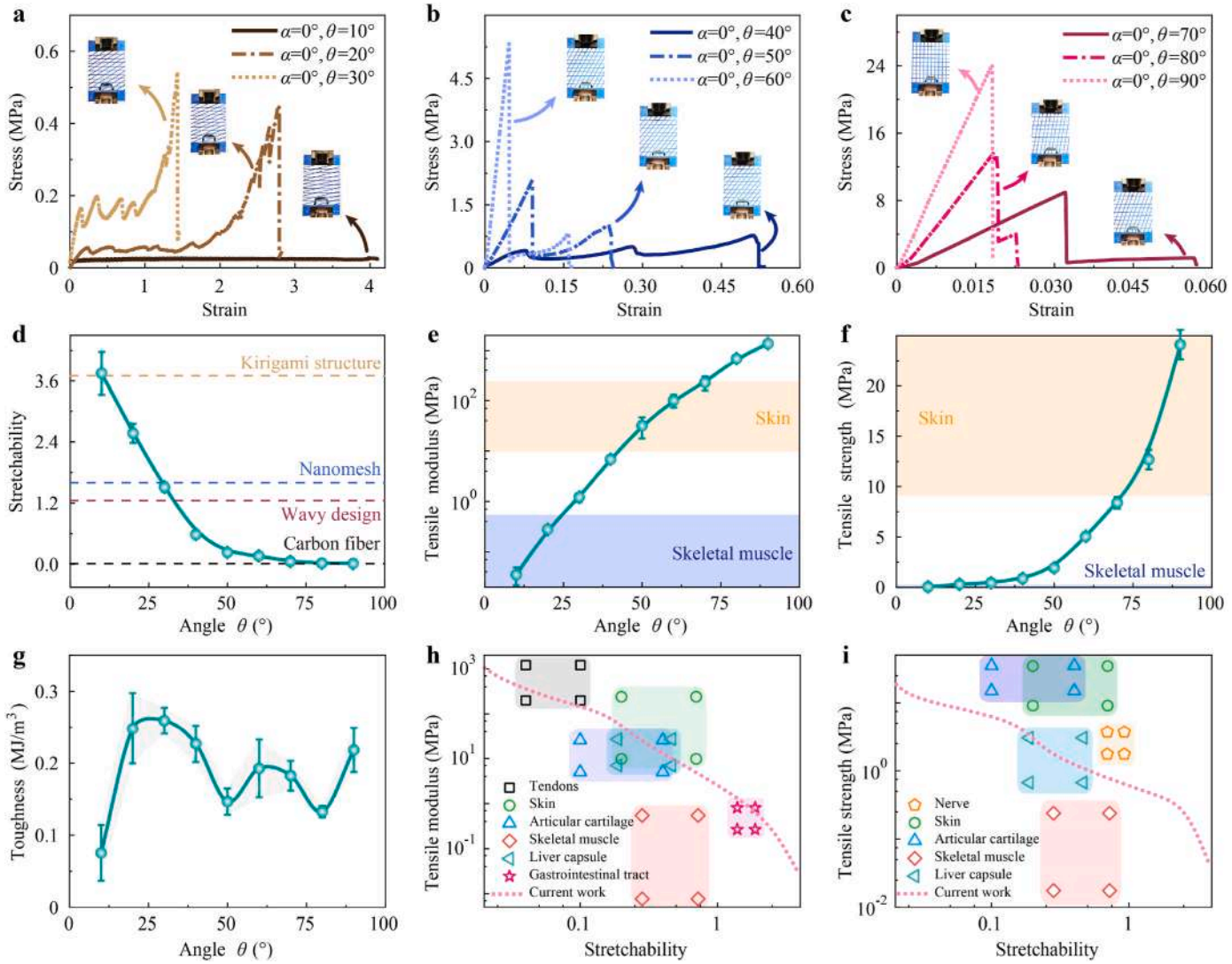

Fig. 2. Structure-based tailorable stretchability and mechanical properties of MCMs. (**a**–**c**) Tensile stress-strain curves of MCMs with constant fiber angle $\alpha = 0°$ and variable fiber angle θ at room temperature (298 K). (**d**) The tailorable stretchability of MCMs with $\alpha = 0°$ compared to other stretchable structures such as wavy structure [31], nanomesh [32] and Kirigami structure [8]. The tunable (**e**) tensile modulus, (**f**) tensile strength and (**g**) toughness of MCMs with $\alpha = 0°$. Where the orange and blue bands represent the range of mechanical properties of skin [33] and skeletal muscle [34], respectively. Material property charts of (**h**) stretchability vs. tensile modulus and (**i**) stretchability vs. tensile strength for natural biomaterials: tendons [35], skin [33] articular cartilage [36], skeletal muscle [34], liver capsule [37], gastrointestinal tract [35] and nerve [38].

stretchability. Therefore, the actual demand on the stretchability and mechanical properties should be weighed when selecting structural parameters. Whether the deformation pattern in the stretched state matches the deformation coordination conditions of the biotic-abiotic interface is one of the key issues that should be considered when designing bio-flexible electronic devices. During the design of MCMs, a lattice cross-lap strategy was employed to eliminate as much as possible the out-of-plane deformation that tends to occur when stretchable structures are stretched in-plane, thus satisfying requirements for smooth surfaces in some flexible devices. As expected, unlike the deformation mode of conventional Kirigami structures whose in-plane stretching is achieved by out-of-plane deformation of thin sheets, MCMs achieve large deformation during in-plane stretching almost exclusively by in-plane elongation and bending of lattices (Fig. S5).

The PLA-based SMP used for the fabrication of MCMs is a thermoplastic polymer with significant temperature-induced variable stiffness capability, thus allowing for tunable stretchability and mechanical properties of MCMs by regulating the temperature. This temperature-based tunable stretchability and mechanical properties of MCMs were investigated by performing uniaxial tensile experiments at various ambient temperatures. As the temperature increases, the stretchability of MCMs is greatly improved, and the stress-strain curves gradually transform into nonlinear J-shaped curves similar to the tensile stress-strain curves of some natural biomaterials (Fig. 3a–c). Of course, the role of temperature in converting the stress-strain curve to a J-shaped curve slowly diminishes with the increase of θ as the elastic carbon fibers gradually dominate the deformation of the structure (Fig. S6). It is observed from Fig. 3d that the J-shaped stress-strain curve of the MCM shifts laterally along the strain axis as θ decreases from 40° to 20° at 338 K. This tunability of the J-shaped curve provides enhanced designability for bio-flexible electronic devices.

Fig. 3e and f illustrate the combined effects of temperature T and structural parameter θ on the stretchability and tensile toughness of MCMs, respectively. On the one hand, the combination of small fiber angle θ and high temperature T leads to large stretchability. On the other hand, the combination of large fiber angle θ and high temperature T ensures high tensile toughness. Fig. 3g indicates that the elevated temperature does not obviously enhance the stretchability of MCMs at $\theta =$

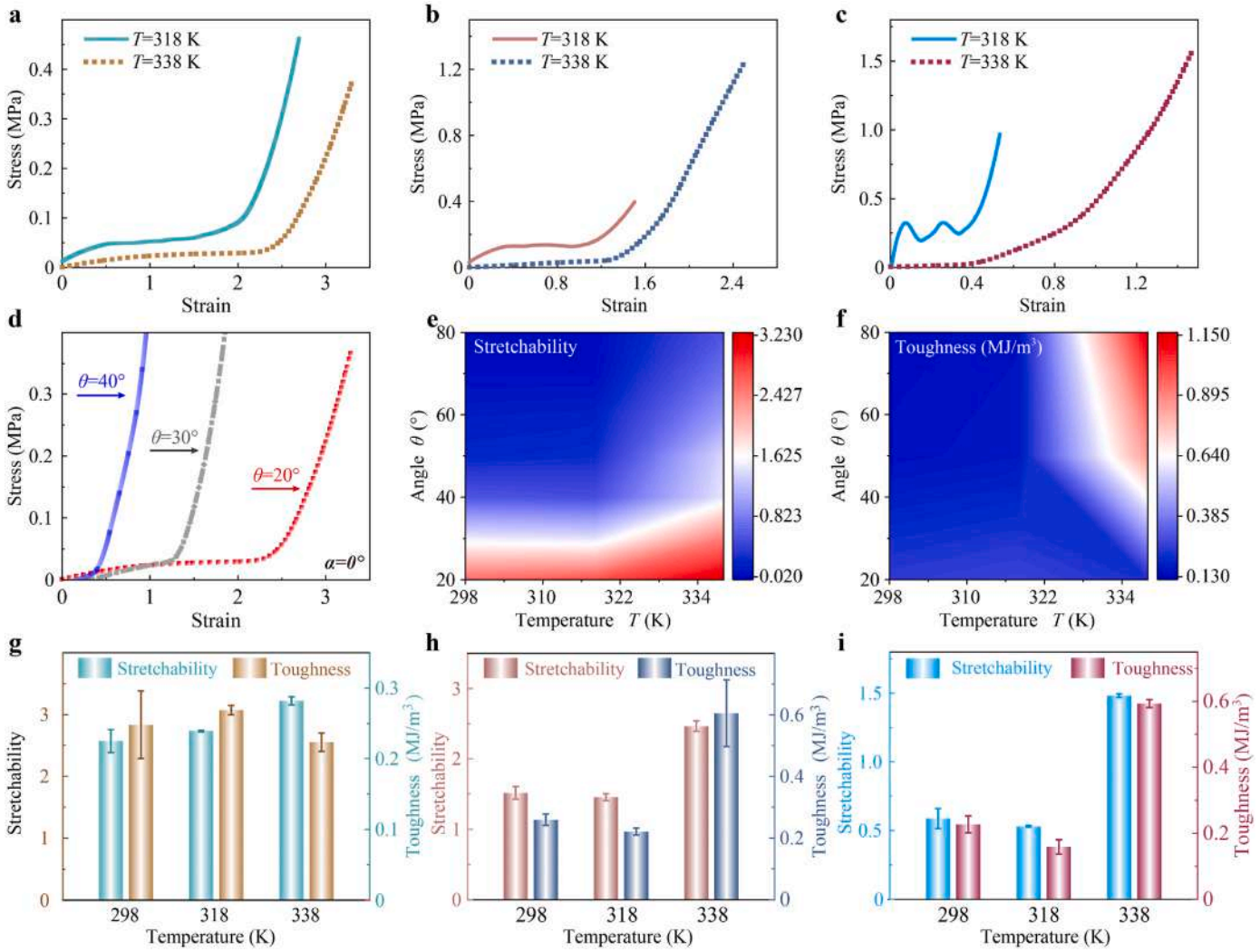

Fig. 3. Temperature-based tunable stretchability and mechanical properties of MCMs. Tensile stress-strain plots for MCMs with (**a**) $\alpha = 0°$, $\theta = 20°$, (**b**) $\alpha = 0°$, $\theta = 30°$ and (**c**) $\alpha = 0°$, $\theta = 40°$ at different temperatures. (**d**) The transverse shift of the stress-strain curve (J-shaped curve) on the strain axis controlled by structural parameters at 338 K. (**e**) Stretchability and (**f**) toughness of MCMs subjected to the combined effects of temperature and θ at $\alpha = 0°$. Temperature-modulated stretchability and toughness of MCMs with (**g**) $\alpha = 0°$, $\theta = 20°$, (**h**) $\alpha = 0°$, $\theta = 30°$ and (**i**) $\alpha = 0°$, $\theta = 40°$.

20°, which is attributed to the large stretching deformation dominated by the geometry. However, the role of temperature in improving the stretchability and tensile toughness of MCMs becomes more significant as θ increases. As shown in Fig. 3h and i, the stretchability of MCMs with $\theta = 30°$ and $\theta = 40°$ respectively increases by 63% and 153% at 338 K compared with that at 298 K, while the corresponding tensile toughness increases by 134% and 162%, respectively. The variation of stretchability and tensile toughness with temperature for MCMs with other θ values are presented in Fig. S7.

3.2. Theoretical simulation on tensile behavior of MCMs

To predict the mechanical behavior and shape memory effect of MCMs, an anisotropic viscoelastic constitutive model of SMPCs was developed (see details in *Supplementary Information*). The model can predict the equivalent viscoelastic stiffness tensor of SMPCs from the stress relaxation modulus of the SMP matrix and elastic constants of fibers. Based on the obtained equivalent stiffness coefficients of SMPCs, the theoretical simulation for the mechanical behavior of 4D printed MCMs was realized by writing a UMAT subroutine of ABAQUS. The model parameter determination is presented in Fig. S8.

The 3D surface and 2D plan plots for the tensile modulus of MCMs at 298 K as a function of fiber angles α and θ obtained by theoretical simulation are presented in Fig. 4a and b, respectively. The preliminary observation that a large α or θ will result in a large tensile modulus is consistent with expectations. Moreover, the effect of θ on the tensile modulus gradually decreases as α increases (Fig. 4c). Fig. 4d and e depict the comparison between experimental measurements and theoretical simulations for the tensile modulus of MCMs with $\alpha = 0°$ at 298 K and 318 K, respectively, from which good agreement is observed. Fig. 4f presents the comparison between the experimental and simulated tensile modulus of MCMs with $\alpha = 30°$ and $\alpha = 60°$. When $\alpha = 60°$, the small θ causes a large difference between the theoretical simulation and experimental measurement of tensile modulus, which is attributed to the large difference between α and θ that causes the fibrous ligament to rotate during the tensile experiment.

To understand the mechanism underpinning the stretchability of MCMs, we investigated the deformation patterns of MCMs subjected to stretching. Fig. S9 presents a comparison between the experimental and simulated deformation process of MCM with $\alpha = 0°$ and $\theta = 40°$, which shows satisfactory agreement. The large deformation of MCMs begins with the tensile-shear coupled deformation of intermediate cells parallel to the fiber angle θ, whose shape changes from rhombic with medium coverage area to hexagonal with high coverage area. As further

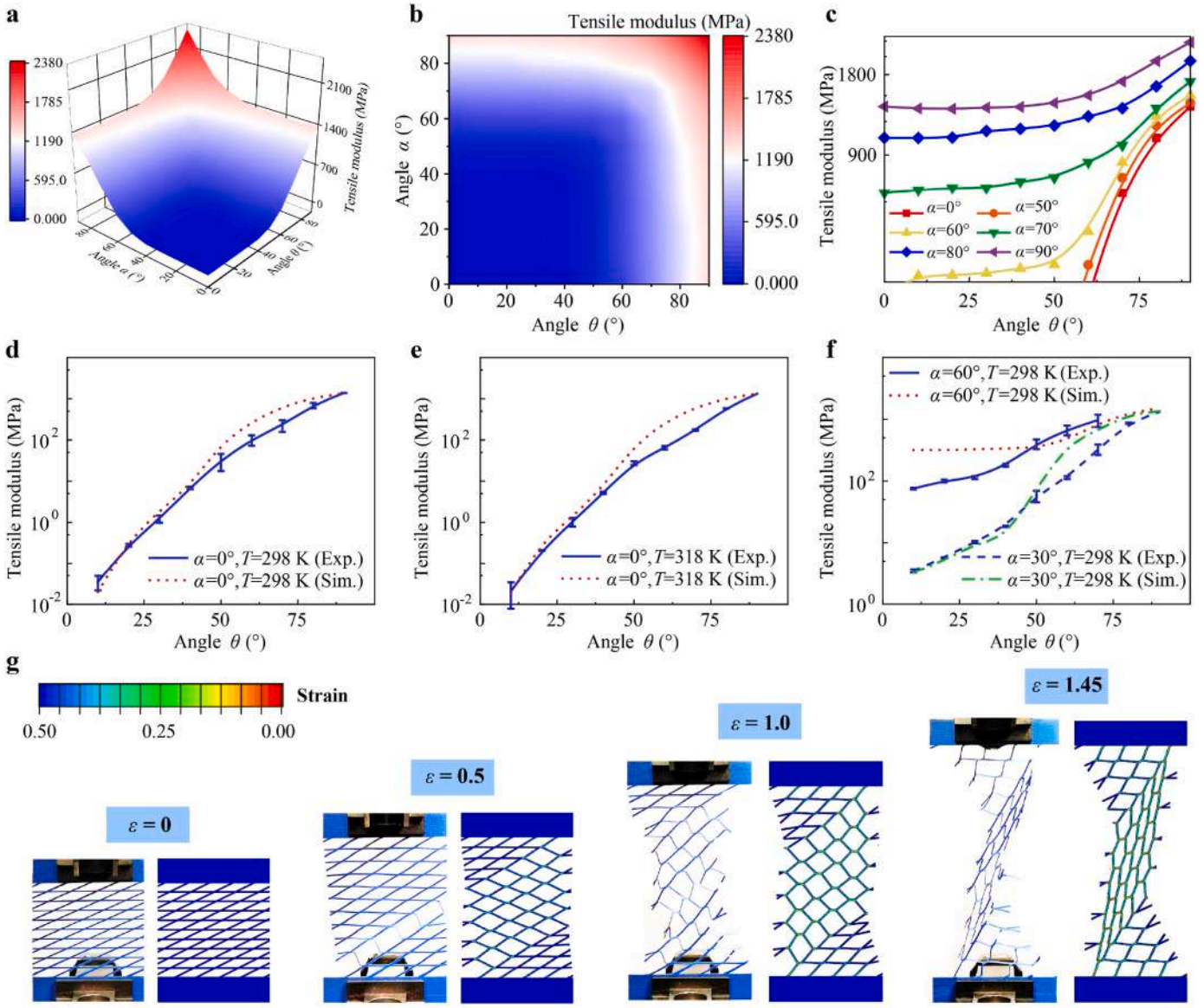

Fig. 4. Theoretical simulations and experimental measurements for the tensile properties of MCMs. (**a**) 3D surface plot and (**b**) 2D plane plot for the tensile modulus of MCMs affected by α and θ at 298 K obtained from simulations. (**c**) The θ - modulus curves obtained by simulations for different α. Comparison of experimental and simulated tensile modulus of MCMs with constant α ($\alpha = 0$) but various θ at (**d**) 298 K and (**e**) 318 K. (**f**) Theoretical simulations and experimental measurements for the tensile modulus of MCMs with $\alpha = 30°$ or $\alpha = 60°$. (**g**) Comparison between experimental and simulated deformation patterns of MCM with $\alpha = 0°$ and $\theta = 30°$ under large stretching.

elongated, hexagonal cells with high coverage area transform to compact quadrilateral cells, accompanied by initial large deformations of their adjacent cells. The above-mentioned deformation mechanism is further confirmed by the tensile deformation process of MCM with $\alpha = 0°$ and $\theta = 30°$ shown in Fig. 4g, where a more pronounced transition from rhombic cells with moderate coverage area to hexagonal cells with high coverage area and then to elongated rectangular cells is observed. It is noteworthy that the ε illustrated in Fig. 4g represents the engineering strain, which is defined in Section 3.1, whereas the strain observed from the finite element cloud maps is the true strain.

When the fiber angle α is not zero, the large deformation mechanism of MCMs is different from the above analysis. Fig. S10 exhibits the deformation process of MCM with $\alpha = 30°$ and $\theta = 40°$, during which cells in the main deformation region always maintain the rhombus shape, and the main change is that their length in the stretching direction gradually increases, while the width in the direction perpendicular to the stretching direction decreases gradually. When MCM is completely symmetrical, such as $\alpha = 30°$ and $\theta = 30°$, the deformation of MCM also exhibits significant symmetry (Fig. S10).

3.3. Shape programmability and reconfigurability of MCMs

Since the matrix material is PLA-based SMP, 4D printed MCMs possess shape memory capability. To verify this capability, shape programming and shape recovery experiments of MCMs were performed. Fig. 5a shows the state of 4D printed MCM in the shape memory cycle obtained by experiments and theoretical simulations. The first three steps of the shape memory cycle (i.e., S1–S3) are defined as the "programming" step, in which MCM is pre-stretched and the temporary shape is fixed. The fourth step (i.e., S4) is a "reconfiguring" step embodying the shape memory effect, in which MCM recovers to its original shape after actively releasing the pre-stretching strain stored during the "programming" process at elevated temperature. By comparing the temporary shape or recovered shape obtained by

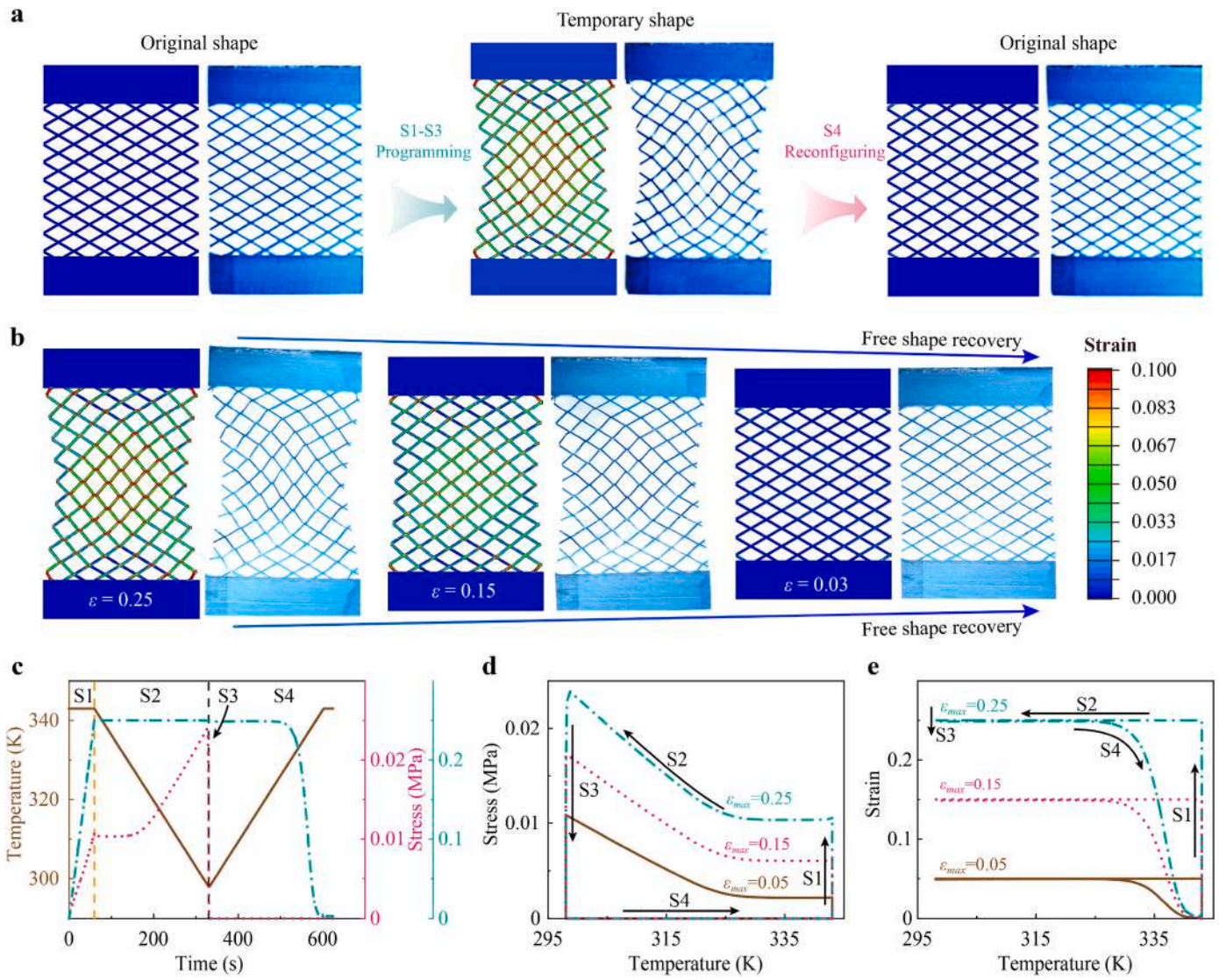

Fig. 5. Shape memory effect of 4D printed MCM. (**a**) Experimental and simulated 4D transformation of MCM from original shape to temporary shape and back again. (**b**) Free shape recovery process of MCM. (**c**) Theoretical simulation for the shape memory cycle. Where S1, S2, S3 and S4 represent the loading phase, the cooling phase, the unloading phase and the heating phase, respectively. (**d**) The temperature-stress curves and (**e**) temperature-strain curves of MCM at different strain levels obtained from theoretical simulations.

experiments and simulations, it is observed that simulations can effectively predict the deformation pattern of MCM in the shape memory cycle. The shape recovery process of MCM with $\alpha = 30°$ and $\theta = 30°$ is given in Fig. 5b, from which it can be found that the shape recovery process of MCM is a pre-strain release process. The pre-strain stored in the temporary shape is concentrated in the middle cells of MCM, so the deformation during the free shape recovery mainly occurs in the parts where these cells are located.

Fig. 5c presents the evolution of temperature, stress, and strain over time for 4D printed MCMs obtained by simulations during shape memory cycling, and the maximum strain applied in step S1 is $\varepsilon_{max} = 0.25$. Steps S1 and S2 are strain control processes, so the strain changes in these steps are linear and predictable, but the stress changes are complex. In step S2, the stress first increases slowly and then increases rapidly as the temperature decreases. SMP has extremely low modulus at high temperatures, so there is little tensile stress due to thermal shrinkage. However, the modulus of SMP becomes larger as the temperature decreases, so the tensile stress caused by thermal contraction gradually increases. Steps S3 and S4 are the load control process, and the strain undergoes a slight attenuation in step S3, which indicates that the shape fixed ratio of MCM is lower than 100%. In step S4, the strain curve shows an inverse S-shape evolution pattern with increasing temperature, and the rapid shape recovery occurs mainly near the glass transition temperature of SMP (328 K–343 K).

According to the above analysis, the relationship between temperature and stress or strain during shape memory cycling is further considered. As can be seen from Fig. 5d, the main difference in the stress versus temperature profiles for different maximum strains ε_{max} originates from the difference in the maximum stress in step S1. In fact, SMP exhibits rubber elasticity at high temperatures, so the stress of MCM at high temperatures increases with the increase of the maximum strain. Nonlinear changes of strain curves mainly occur in step S4, which is a free shape recovery process (Fig. 5e). When the temperature is lower than 328 K, the strain hardly changes with the increase of temperature. However, a fast shape recovery response is observed when the temperature is raised to 328 K, and the strain gradually approaches zero with increasing temperature.

3.4. MCM-based stretchable LED integrated system

4D printed MCMs have promising applications in the field of flexible electronics due to their high stretchability and tunable mechanical properties matched with biomaterials. Fig. 6 shows the composition and application demonstration of a stretchable LED electronic device based on 4D printed MCM. The device consists of an MCM substrate, several LEDs, a conductive silver film after silver paste curing, and an external DC power supply device (Fig. 6a). Here, the conductive silver film scarcely alters the overall mechanical properties of the MCM substrate because its thickness is several orders of magnitude smaller than the thickness of the MCM substrate. Moreover, the true strain in the MCM substrate during stretching is extremely low, and therefore does not lead to widespread failure of the conductive silver film.

To verify the stretchability of the LED electronic device, the device is stretched in the energized state and the resistance change during stretching is recorded. Fig. 6b presents the optical images of the LED electronic device before being stretched and at a strain of 10%. Three LEDs always remain sufficiently bright without appreciably sacrificing light intensity. Furthermore, the resistance of the device during stretching is maintained at about 60 Ω without significant resistance fluctuations, which ensures stable electrical properties of the device (Fig. 6c). In addition, mechanical properties compatible with biomaterials such as human skin can be obtained by adjusting structural parameters of 4D printed MCM, so the stretchable LED electronic demonstrated here can be used for health monitoring during human exercise instead of some traditional electronic devices with complex compositions (Fig. 6d). It is worth noting that the prospect of 4D printed MCMs in the field of flexible electronics is not limited to LED circuits. The LEDs shown here can also be replaced by other electronic components that are widely used in stretchable devices and systems.

4. Conclusions

In conclusion, we introduce 4D printing technology to fabricate bio-inspired MCMs with excellent mechanical properties and high stretchability. The stretchability of MCMs can be adjusted in the range of 1.8%–375% and the tensile modulus of MCMs can be customized in the range of 0.04 MPa–1375 MPa by controlling the orientation of fibrous ligaments, resulting in mechanical properties similar to those of various biological tissues such as skin and skeletal muscle. The large stretchability of MCMs is caused by in-plane tensile-bending coupled deformation of fibrous ligaments, accompanied by rotation of fibrous ligaments. Such a large deformation characteristic is highly desirable for stretchable devices requiring smooth deformation surfaces and low surface roughness such as flexible transparent electrodes. Through experimental analysis and theoretical simulations, we further validate the shape programmability and reconfigurability of 4D printed MCMs, and these unique properties enable the design of actively stretchable flexible electronics. For instance, by applying a pre-stretch strain to the MCM at elevated temperatures and then cooling to fix the deformation, the pre-stretched MCM will exhibit mechanical properties at room temperature that differ from those of an unstretched MCM. Consequently, when 4D printed MCMs are utilized as flexible electronic devices, they can be pre-stretched to align their mechanical properties with specific application demands. Moreover, they can exploit the shape memory effect to recover from a pre-stretched state to their original unstretched state. To demonstrate potential applications, we design a stretchable LED electronic device based on 4D printed MCM that retains electronic conductivity under large stretching. The proposed design and fabrication strategies for stretchable mesh composites have general utility in various flexible electronics technologies and thus exhibit broad application prospects in designing actively flexible stretchable devices

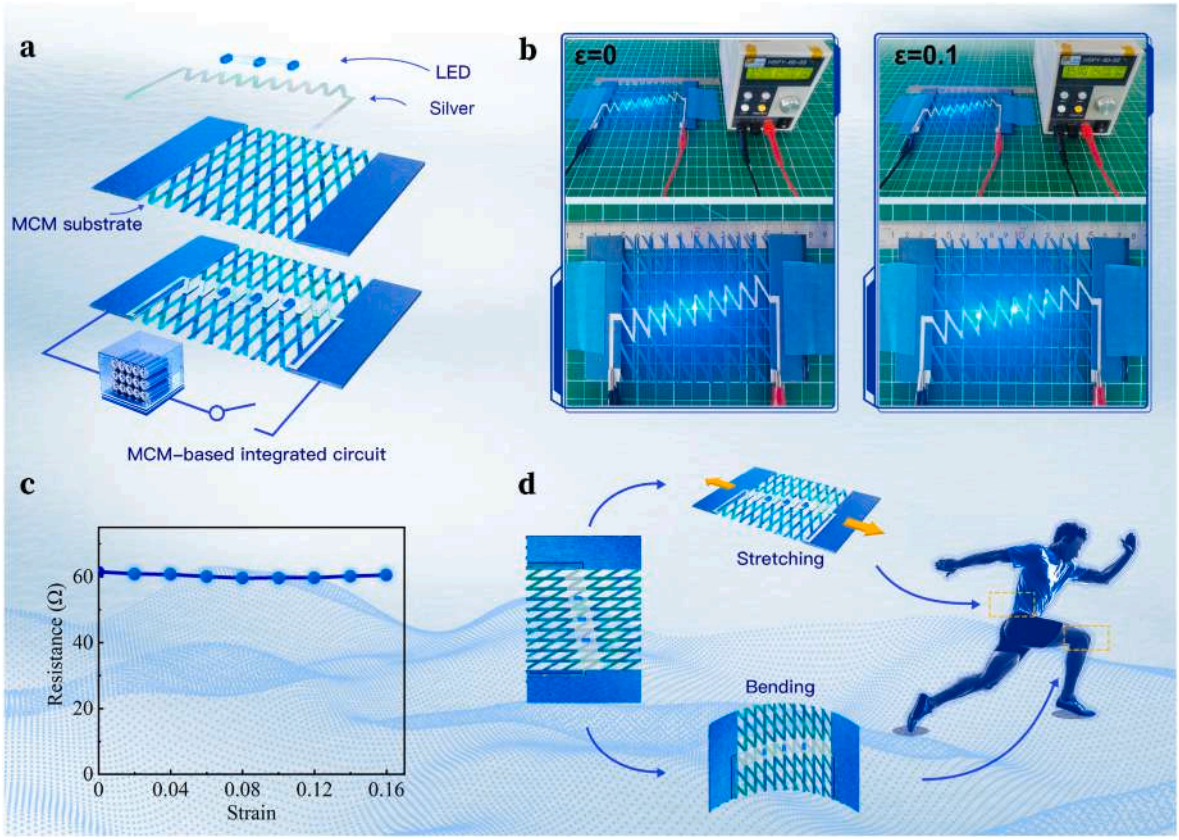

Fig. 6. Demonstration of 4D printed MCMS in stretchable LED electronics. (**a**) The decomposition view and circuit diagram of stretchable LED electronics. (**b**) Optical images of manipulated LED electronics before and after stretching. (**c**) Relationship between the resistance of LED electronics and the applied strain during uniaxial stretching. (**d**) Demonstration of stretchable electronics in human motion monitoring.

with different target applications.

CRediT authorship contribution statement

Chengjun Zeng: Funding acquisition, Investigation, Methodology, Visualization, Writing – original draft, Writing – review & editing. **Liwu Liu:** Conceptualization, Formal analysis, Funding acquisition. **Xiaozhou Xin:** Methodology, Validation. **Wei Zhao:** Data curation, Validation. **Cheng Lin:** Investigation, Writing – review & editing. **Yanju Liu:** Funding acquisition, Supervision, Writing – review & editing. **Jinsong Leng:** Project administration, Supervision.

Declaration of competing interest

The authors declare that they have no known competing financial interests or personal relationships that could have appeared to influence the work reported in this paper.

Data availability

Data will be made available on request.

Acknowledgments

This work was financially supported by the National Natural Science Foundation of China (Grant Nos. 12072094 and 12172106), the China Postdoctoral Science Foundation (Grant No. 2023M730870), the Postdoctoral Fellowship Program of CPSF (Grant No. GZB20230957) and the Heilongjiang Postdoctoral Science Foundation (Grant No. LBH-Z23130).

Appendix A. Supplementary data

Supplementary data to this article can be found online at https://doi.org/10.1016/j.compscitech.2024.110503.

References

[1] Y. Qu, X. Li, X. Wang, H. Dai, Multifunctional AgNWs@MXene/AgNFs electromagnetic shielding composites for flexible and highly integrated advanced electronics, Compos. Sci. Technol. 230 (2022) 109753.
[2] V. Orts Mercadillo, K.C. Chan, M. Caironi, A. Athanassiou, I.A. Kinloch, M. Bissett, P. Cataldi, Electrically conductive 2D material coatings for flexible and stretchable electronics: a comparative review of graphenes and MXenes, Adv. Funct. Mater. 32 (2022) 2204772.
[3] L. Hu, P.L. Chee, S. Sugiarto, Y. Yu, C. Shi, R. Yan, Z. Yao, X. Shi, J. Zhi, D. Kai, H. D. Yu, W. Huang, Hydrogel-based flexible electronics, Adv. Mater. 35 (14) (2023) e2205326.
[4] H. Li, H. Liu, M. Sun, Y. Huang, L. Xu, 3D interfacing between soft electronic tools and complex biological tissues, Adv. Mater. 33 (3) (2021) e2004425.
[5] L. Veeramuthu, C.J. Cho, F.C. Liang, M. Venkatesan, G.R. Kumar, H.Y. Hsu, R. J. Chung, C.H. Lee, W.Y. Lee, C.C. Kuo, Human skin-inspired electrospun patterned robust strain-insensitive pressure sensors and wearable flexible light-emitting diodes, ACS Appl. Mater. Interfaces 14 (26) (2022) 30160–30173.
[6] M. Sang, K. Kim, J. Shin, K.J. Yu, Ultra-thin flexible encapsulating materials for soft bio-integrated electronics, Adv. Sci. 9 (30) (2022) e2202980.
[7] L. Yin, J. Lv, J. Wang, Structural innovations in printed, flexible, and stretchable electronics, Adv. Mater. Technol. 5 (11) (2020) 2000694.
[8] C. Wang, C. Wang, Z. Huang, S. Xu, Materials and structures toward soft electronics, Adv. Mater. 30 (50) (2018) e1801368.
[9] X. Ye, X. Meng, Z. Han, Y. Qi, Z. Li, P. Tian, W. Wang, J. Li, Y. Li, W. Zhang, R. Yang, Designing Fe-containing polyhedral oligomeric silsesquioxane to endow superior mechanical and flame-retardant performances of polyamide 1010, Compos. Sci. Technol. 233 (2023) 109894.
[10] H. Cho, B. Lee, D. Jang, J. Yoon, S. Chung, Y. Hong, Recent progress in strain-engineered elastic platforms for stretchable thin-film devices, Mater. Horiz. 9 (2022) 2053.
[11] J. Dong, G. Ye, Y. Wang, F. Jin, H. Fan, Design, manufacture and crushing behaviors of buckling-inspired auxetic meta-lattice structures, Int. J. Smart Nano Mater. 12 (4) (2021) 491–510.
[12] T.S.D. Le, H.P. Phan, S. Kwon, S. Park, Y. Jung, J. Min, B.J. Chun, H. Yoon, S.H. Ko, S.W. Kim, Y.J. Kim, Recent advances in laser-induced graphene: mechanism, fabrication, properties, and applications in flexible electronics, Adv. Funct. Mater. 32 (48) (2022) 2205158.
[13] P. Liu, N. Sun, Y. Mi, X. Luo, X. Dong, J. Cai, X. Jia, M.A. Ramos, T.S. Hu, Q. Xu, Ultra-low CNTs filled high-performance fast self-healing triboelectric nanogenerators for wearable electronics, Compos. Sci. Technol. 208 (2021) 108733.
[14] J. Chen, L. Zhang, Y. Tu, Q. Zhang, F. Peng, W. Zeng, M. Zhang, X. Tao, Wearable self-powered human motion sensors based on highly stretchable quasi-solid state hydrogel, Nano Energy 88 (2021) 106272.
[15] T. Ding, Y. Zhou, X.Q. Wang, C. Zhang, T. Li, Y. Cheng, W. Lu, J. He, G.W. Ho, All-soft and stretchable thermogalvanic gel fabric for antideformity body heat harvesting wearable, Adv. Energy Mater. 11 (2021) 2102219.
[16] J.C. Yang, S. Lee, B.S. Ma, J. Kim, M. Song, S.Y. Kim, D.W. Kim, T.S. Kim, S. Park, Sci. Adv. 8 (2022) eabn3863.
[17] Z. Xue, H. Song, J.A. Rogers, Y. Zhang, Y. Huang, Mechanically-guided structural designs in stretchable inorganic electronics, Adv. Mater. 32 (15) (2020) e1902254.
[18] S. Huang, Y. Liu, Y. Zhao, Z. Ren, C.F. Guo, Flexible electronics: stretchable electrodes and their future, Adv. Funct. Mater. 29 (6) (2018) 1805924.
[19] A.K. Brooks, S. Chakravarty, M. Ali, V.K. Yadavalli, Kirigami-inspired biodesign for applications in healthcare, Adv. Mater. 34 (18) (2022) e2109550.
[20] M. Karami-Mosammam, D. Danninger, D. Schiller, M. Kaltenbrunner, Stretchable and biodegradable batteries with high energy and power density, Adv. Mater. 34 (2022) e2204457.
[21] B. Yiming, L. Wu, M. Zhang, Z. Han, P. Zhao, T. Li, Z. Jia, S. Qu, Highly stretchable bilayer lattice structures that elongate via in-plane deformation, Adv. Funct. Mater. 30 (12) (2020) 1909473.
[22] Y. Zhou, Y. Yang, A. Jian, T. Zhou, G. Tao, L. Ren, J. Zang, Z. Zhang, Co-extrusion 4D printing of shape memory polymers with continuous metallic fibers for selective deformation, Compos. Sci. Technol. 227 (2022) 109603.
[23] C.A. Spiegel, M. Hackner, V.P. Bothe, J.P. Spatz, E. Blasco, 4D printing of shape memory polymers: from macro to micro, Adv. Funct. Mater. 32 (2022) 2110580.
[24] W. Peng, J. Yin, X. Zhang, Y. Shi, G. Che, Q. Zhao, J. Liu, 4D printed shape memory anastomosis ring with controllable shape transformation and degradation, Adv. Funct. Mater. 33 (20) (2023) 2214505.
[25] Y. Wang, J. Jin, Y. Lu, D. Mei, 3D printing of liquid metal based tactile sensor for simultaneously sensing of temperature and forces, I, Int J. Smart Nano. Mater. 12 (2021) 269–285.
[26] H. Ren, X. Yang, Z. Wang, X. Xu, R. Wang, Q. Ge, Y. Xiong, Smart structures with embedded flexible sensors fabricated by fused deposition modeling-based multimaterial 3D printing, Int. J. Smart Nano Mater. 13 (3) (2022) 447–464.
[27] Y.F. Zhang, Z. Li, H. Li, H. Li, Y. Xiong, X. Zhu, H. Lan, Q. Ge, Fractal-based stretchable circuits via electric-field-driven microscale 3D printing for localized heating of shape memory polymers in 4D printing, ACS Appl. Mater. Interfaces 13 (35) (2021) 41414–41423.
[28] Y. Zhou, C.B. Parker, P. Joshi, A.K. Naskar, J.T. Glass, C. Cao, 4D printing of stretchable supercapacitors via hybrid composite materials, Adv. Mater. Technol. 6 (1) (2020) 2001055.
[29] E.A. Zimmermann, E. Schaible, B. Gludovatz, F.N. Schmidt, C. Riedel, M. Krause, E. Vettorazzi, C. Acevedo, M. Hahn, K. Puschel, S. Tang, M. Amling, R.O. Ritchie, B. Busse, Intrinsic mechanical behavior of femoral cortical bone in young, osteoporotic and bisphosphonate-treated individuals in low- and high energy fracture conditions, Sci. Rep. 6 (2016) 21072.
[30] W. Zhang, F. Zhang, X. Lan, J. Leng, A.S. Wu, T.M. Bryson, C. Cotton, B. Gu, B. Sun, T.-W. Chou, Shape memory behavior and recovery force of 4D printed textile functional composites, Compos. Sci. Technol. 160 (2018) 224–230.
[31] H.W. Jang, S. Kim, S.M. Yoon, Impact of polyimide film thickness for improving the mechanical robustness of stretchable InGaZnO thin-film transistors prepared on wavy-dimensional elastomer substrates, ACS Appl. Mater. Interfaces 11 (37) (2019) 34076–34083.
[32] C.F. Guo, T. Sun, Q. Liu, Z. Suo, Z. Ren, Highly stretchable and transparent nanomesh electrodes made by grain boundary lithography, Nat. Commun. 5 (2014) 3121.
[33] M. Ottenio, D. Tran, A. Ni Annaidh, M.D. Gilchrist, K. Bruyere, Strain rate and anisotropy effects on the tensile failure characteristics of human skin, J. Mech. Behav. Biomed. Mater. 41 (2015) 241–250.
[34] D.A. Morrow, T.L. Haut Donahue, G.M. Odegard, K.R. Kaufman, Transversely isotropic tensile material properties of skeletal muscle tissue, J. Mech. Behav. Biomed. Mater. 3 (1) (2010) 124–129.
[35] D. Wang, Y. Xiong, B. Zhang, Y.F. Zhang, D. Rosen, Q. Ge, Design framework for mechanically tunable soft biomaterial composites enhanced by modified horseshoe lattice structures, Soft Matter 16 (6) (2020) 1473–1484.
[36] F.T. Moutos, L.E. Freed, F. Guilak, A biomimetic three-dimensional woven composite scaffold for functional tissue engineering of cartilage, Nat. Mater. 6 (2) (2007) 162–167.
[37] A. Brunon, K. Bruyere-Garnier, M. Coret, Mechanical characterization of liver capsule through uniaxial quasi-static tensile tests until failure, J. Biomech. 43 (11) (2010) 2221–2227.
[38] G.H. Borschel, K.F. Kia, W.M. Kuzon, R.G. Dennis, Mechanical properties of acellular peripheral nerve, J. Surg. Res. 114 (2) (2003) 133–139.